β decay of ^{78}Sr

A. B. Pérez-Cerdán,[1] B. Rubio,[1,*] W. Gelletly,[2] A. Algora,[1] J. Agramunt,[1] K. Burkard,[3] W. Hüller,[3] E. Nácher,[1,4] P. Sarriguren,[4] L. Caballero,[1] F. Molina,[1] L. M. Fraile,[5] E. Reillo,[4] M. J. G. Borge,[4] Ph. Dessagne,[6] A. Jungclaus,[4] and M.-D. Salsac[6]

[1]*Instituto de Física Corpuscular, CSIC-Universitat de Valencia, E-46071 Valencia, Spain*
[2]*Department of Physics, University of Surrey, Guildford GU2 5XH, United Kingdom*
[3]*Gesellschaft für Schwerionenforschung mbH, D-64291 Darmstadt, Germany*
[4]*Instituto de Estructura de la Materia, CSIC, E-28006 Madrid, Spain*
[5]*Grupo de Física Nuclear, Universidad Complutense, E-28040 Madrid, Spain*
[6]*Institut Pluridisciplinaire Hubert Curien, IN$_2$P$_3$-CNRS, F-67037 Strasbourg, Cedex2, France*

(Received 15 June 2011; revised manuscript received 8 September 2011; published 16 November 2011)

The γ rays and conversion electrons emitted in the β decay of ^{78}Sr to levels in ^{78}Rb have been studied using Ge detectors and a mini-orange spectrometer. A reliable level scheme based on the results of these experiments has been established. The properties of the levels in ^{78}Rb have been compared with calculations based on deformed Hartree-Fock with Skyrme interactions and pairing correlations in the BCS approximation. This has allowed an interpretation of the nature of the observed sets of levels in the odd-odd nucleus ^{78}Rb.

DOI: 10.1103/PhysRevC.84.054311 PACS number(s): 23.40.−s, 21.60.Ev, 23.20.Lv, 27.50.+e

I. INTRODUCTION

The nuclei with mass $A = 70$–80 close to the $N = Z$ line have provided a happy hunting ground for nuclear spectroscopists and theorists for some time [1]. The fact that the protons and neutrons are filling the same shells and that there are energy gaps at nucleon numbers 34, 36, 38, and 40 leads to a landscape where nuclear properties change rapidly with the addition or subtraction of a single nucleon. Thus, the nuclear shape may change from nucleus to nucleus. We also find shape coexistence in these nuclei with oblate, spherical, and prolate shapes all competing in terms of excitation energy. Such nuclei are also of interest because it is here that we might hope to observe the effects of neutron-proton pairing, an effect that is washed out by the much larger number of like-nucleon pairs as we move away from the $N = Z$ line.

The variation in shape along the $N = Z$ line has been explored [2,3] and we see a steady change as we go from ^{64}Ge toward ^{100}Sn with a peak in deformation at ^{76}Sr and ^{80}Zr in the middle of the shell as one might expect from simple parametrizations such as the P scheme of Casten *et al.* [4–6]. Shape co-existence was first reported by Piercey *et al.* [7] in the Se isotopes as early as 1981. More recently, studies of isomeric decays produced following fragmentation [8] and subsequent measurements of the Coulomb excitation of beams of radioactive ^{74}Kr and ^{72}Kr [9,10] have shown that there are low-lying, excited 0^+ states in these nuclei. The mixing of these states with the ground state could be extracted in terms of simple two-level mixing [11].

Studies of β decay have also been used to extract similar information. It was suggested by Hamamoto *et al.* [12] and followed up by Sarriguren *et al.* [13] that the shape of the β strength function is sensitive to the deformation of the parent nucleus. This has been confirmed experimentally [14,15] in studies using the total absorption spectroscopy (TAS) method [16].

This rich diversity of shape and behavior has attracted considerable attention from theorists, who have applied a variety of different approaches to try to explain what we observe. These include *inter alia* calculations in the configuration-dependent shell correction approach with deformed Woods-Saxon potentials [17], self-consistent deformed Skyrme mean-field calculations [18,19], Hartree-Fock-Bogoliubov calculations with the Gogny force [20], relativistic mean-field calculations [21], and the self-consistent complex excited VAMPIR model [22].

In the present work we are concerned with the β^+/EC decay of ^{78}Sr to levels in ^{78}Rb. This is part of a program of measurements aimed at establishing nuclear shapes using the TAS method [14,15]. To analyze the data from the TAS spectrometer we require some knowledge of the low-lying part of the level scheme in the daughter nucleus. Moreover, the better our knowledge of the level scheme the higher is the accuracy that can be achieved in evaluating the total absorption data. Accordingly, as well as studying ^{78}Sr decay with the TAS spectrometer Lucrecia [16] at ISOLDE, we have also studied the γ rays and conversion electrons emitted in this decay using Ge detectors and a mini-orange spectrometer to establish a reliable decay scheme for this nucleus. At the same time the study of discrete levels in ^{78}Rb populated in the decay of ^{78}Sr can help us to understand the structure of the daughter nucleus better. The aim of the present paper is to report on these high-resolution studies of the decay of ^{78}Sr. The results from the TAS study will be reported in a separate paper.

There appears to have been only two previous studies [23,24] of the β^+/EC decay of ^{78}Sr. The more comprehensive of the two is the work of Mukai *et al.* [24]. They studied γ-ray singles and coincidence spectra in the ^{78}Sr β decay and also studied the in-beam γ rays from the ^{54}Fe(^{28}Si, $3pn$)^{78}Rb reaction. They constructed a simple decay scheme showing

*berta.rubio@ific.uv.es

six excited states in ^{78}Rb populated in the decay. Their short paper indicates that the 5.74-min isomeric state in ^{78}Rb at 111.2 keV excitation energy was populated directly in their study because they observed that the measured decay curve for the 103.2-keV γ ray is influenced by its being populated in the isomeric decay as well as in ^{78}Sr decay. They were not able to see the linking transition from the isomer. This was later observed by McNeill *et al*. [25] and the excitation energy of the isomer determined. Since then a number of in-beam studies have been carried out. The most complete of these is reported by Kaye *et al*. [26,27]. They report nine bands based on low-lying levels and also provide information on some of the levels at low spin which are populated in ^{78}Sr decay.

In the present paper we report the results of our experimental investigation of the decay of ^{78}Sr and the level structure of ^{78}Rb. The measured levels are compared with and interpreted in terms of microscopic calculations based on deformed Hartree-Fock with Skyrme interactions and pairing correlations in the BCS approximation [28]. Although these calculations should not be taken literally in terms of the excitation energies associated with particular configurations, they can be taken as a guide to the interpretation of the nature of the observed states if we characterize them in terms of I^{π} assignments.

II. EXPERIMENTS

Measurements of the β-delayed γ rays and conversion electrons emitted in the β^+/EC decay of ^{78}Sr were made at CERN-ISOLDE. Two separate experiments were carried out at different times. They are described below.

In both cases the Sr nuclei were produced in a Nb target of thickness 37 g cm^{-2} with a beam of 1.4-GeV protons from the PS Booster accelerator. The PS Booster delivers pulses of 3.2×10^{13} protons per pulse every 1.2 s. Each pulse lasts for 2.4 μs. At the time of this experiment the pulses were organized in a supercycle of 14 pulses with the flexibility to deliver a varying sequence and number of pulses to ISOLDE and other facilities. In the experiments described here different numbers and sequences of pulses in the supercycle were used. The ions were produced in a surface ion source made of tungsten. To suppress the isobaric reaction products, particularly Rb ions, which are produced in much greater abundance, CF_4 was added to the ion source carrier gas [29]. This allowed one to extract SrF^+ ions from the ion source at 60 keV [30]. They were mass analyzed in the general purpose separator (GPS) and directed into the beam line, which carries them to the experimental apparatus. No evidence of any contamination of the Sr beam, particularly no Rb, was observed in our experiments. The two measurements are described in the following sections.

A. γ-ray studies

The setup used in the first experiment is shown schematically in Fig. 1.

Here the radioactive SrF^+ ions were implanted upstream from the measuring point in a tape which could be moved after a fixed time to carry the accumulated activity to the counting position and, at the same time, remove the residual activity.

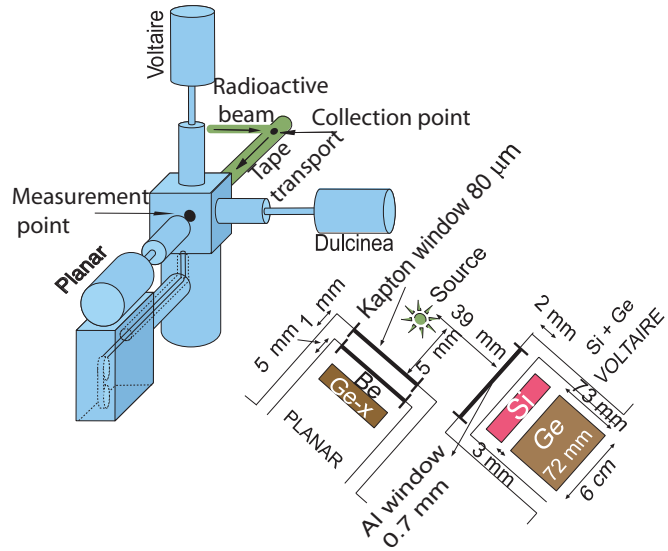

FIG. 1. (Color online) A sketch of the experimental setup for the γ-ray singles and γ-γ and γ-x-ray coincidences (see Sec. II A of text). On the top left we see the geometry with the three Ge detectors, all at 90° to one another. On the bottom right we see a vertical cross section through the apparatus. The figure is not to scale but the thicknesses of the various windows, the dimensions of the planar and Voltaire detectors, and the distances from the source to the detectors are marked. It should be noted that Voltaire consists of a Si detector in front of a 70% efficiency Ge coaxial detector.

In this experiment a symmetric cycle was used in which the collection of the source and simultaneous measurement of the activity was 231 s. This is approximately one and a half times the half-life of ^{78}Sr and is a compromise between the fraction of the saturation activity reached and the counting time. It also fits with the structure of the pulses in the supercycle of the PS-Booster accelerator, which provides the primary proton beam. Together with the 4 s used in moving the tape this equals the 235.2-s overall length of the supercycle. The activity of the source after the collection was ~12.7 kBq and the beam gate used 100 ms. As can be seen in Fig. 1 the γ rays from the source can be detected by three detectors, which are placed at right angles to each other. The geometry was chosen to minimize the possibility of coincidences between the annihilation quanta. One of the detectors is a planar Ge detector of 14 mm thickness and a front face of 35.7 mm diameter with a Be window of 300 μm thickness. It has an energy resolution of 0.6 keV at 121.8 keV. The other two are coaxial Ge detectors of 40% (Dulcinea) and 70% (Voltaire) efficiency with an energy resolution of 1.6 and 2.0 keV, respectively, at 121.8 keV. Voltaire also has a Si detector of 300 μm thickness in front of the Ge detector with a separation of 3 mm between the two. Figure 1 shows the various distances from the source to the detector front faces as well as the thicknesses of the windows in front of the detectors and other dimensions. These numbers are important to allow us to perform Monte Carlo simulations of summing effects in the Ge detectors. Both singles and γ-ray coincidences were recorded. The coincidence requirement was that two of the three detectors fired within a coincidence gate of 250 ns.

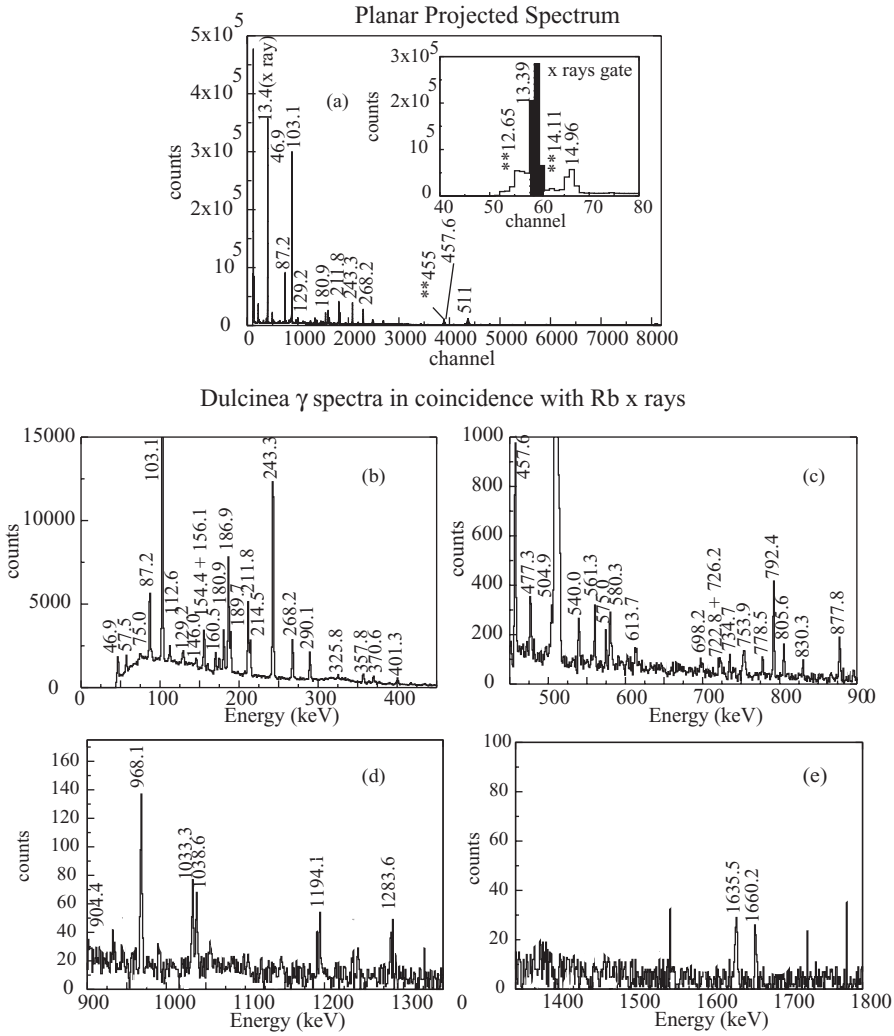

FIG. 2. In the top panel of the figure is shown a projected spectrum of the γ rays observed in the planar detector. The peaks are labeled with their energies in keV. Those marked ** are from the decay of the daughter nucleus ^{78}Rb. The inset indicates the gate set on the Rb x rays, which reveals the coincident γ-ray spectrum in Dulcinea shown below. Some random spikes appear on the projected spectrum owing to a nonperfect background subtraction. They do not correspond to any γ ray in ^{78}Rb and are therefore not labeled. Note that the spectrum from Dulcinea is plotted in sections, which are continuations of one another.

In an experiment with a target-ion source of this type the yield of ions with a fixed primary beam current generally decreases as a function of time. In this experiment in the early stages of the life of the target-ion source four of the pulses from the PS Booster supercycle delivered sources that resulted in counting rates of 15 and 4.5 kBq in the planar detector and Voltaire, respectively. The coincidence counting rate was 2.4 kBq. The data acquisition system was inhibited for 10 ms after each impact of the PS Booster beam on the target to eliminate any background from neutrons or γ rays generated in the ISOLDE target. Overall, this measurement lasted approximately 8 h and the source activity was essentially constant over this time scale. Afterward the detectors were calibrated for efficiency and energy using standard sources of ^{241}Am, ^{133}Ba, and ^{152}Eu. Figures 2 and 3 show examples of the recorded coincidence spectra from the planar and Dulcinea detectors.

B. The half-life of ^{78}Sr

The half-life of ^{78}Sr decay was determined in the experiment described in the previous section and with the setup shown in Fig. 1. The singles γ-ray spectra in the planar detector were recorded with a time stamp that was reset after each tape movement. The step time of the clock used was 65 ms. The data were divided into time bins corresponding to 20 steps of the clock. The peak area of the strong 103.1-keV transition was measured for each bin. The resulting curve of the peak area versus time measured with the planar detector, shown in Fig. 4, was fitted with an exponential function and a value of 155(3) s was obtained for the half-life. This agrees with the values of 150(20) s, 170(30) s, and 159(8) s given by Liang *et al.* [31], Hagebø *et al.* [32], and Grawel *et al.* [23], respectively.

C. Internal conversion studies

To determine the multipolarities of the β-delayed transitions assigned to ^{78}Rb, a second experiment was carried out to measure their internal conversion coefficients. The measurements were made with a mini-orange spectrometer constructed and used by Barden at the GSI mass separator. It is described in detail in his thesis [33] and briefly in the Appendix to this paper.

In the present set of measurements only one type of magnet was used, namely, the B type shown in Fig. 9 in the Appendix. Spectra were acquired with four different combinations of magnets and distances. The top four panels of Fig. 5 show

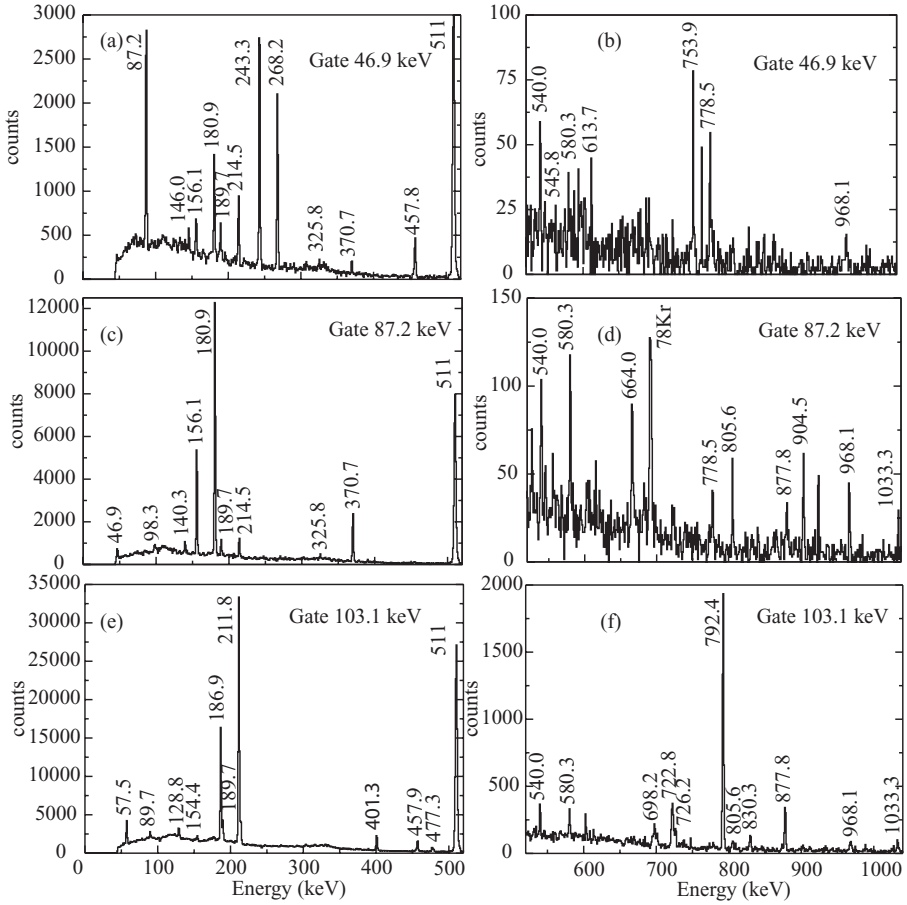

FIG. 3. Projection of the spectra in Dulcinea obtained by gating on the 46.9-keV (a),(b), 87.2-keV (c),(d), and 103.1-keV transitions (e),(f) in the planar detector. The peak labeled ^{78}Kr in (d) is the 693-keV line in ^{78}Kr. This line is in coincidence with Kr x rays and a previously unreported 87-keV transition in ^{78}Rb decay.

the measured transmission curves for these four arrangements. The transmission curves were obtained by measuring the well-known lines from open standard sources of ^{133}Ba and ^{152}Eu and also lines of known relative intensity from the decay of ^{77}Rb, ^{79}Sr, and ^{79}Rb [34–36] produced from the GPS in the same way as the ^{78}Sr sources under study. The bottom part of Fig. 5 shows an example of a conversion electron spectrum recorded with the 6/8/125 combination. Each of the lines is marked with the energy of the electromagnetic transition and the shell in which conversion occurred.

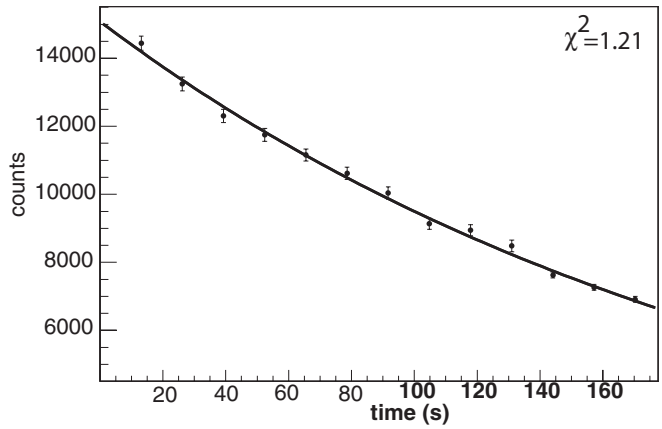

FIG. 4. A plot of the peak area of the strong 103-keV γ ray as a function of time measured with the planar detector. The line indicates the best mean-square fit to the data and the reduced χ^2 obtained. This leads to a half-life of 155(3) s for ^{78}Sr (see Sec. II B of the text). Fits to peak areas of weaker γ lines in the ^{78}Sr decay are consistent with this value.

In this second experiment a Ge telescope was placed at 180° to the mini-orange. This telescope consists of a planar Ge of 10 mm thickness and a front face of 50.5 mm diameter with a coaxial detector of 20% efficiency placed 12 mm behind it. This telescope has a Be window of 300 μm thickness in front of it to allow low-energy photons to enter with the minimum absorption. In addition to the telescope a 70% efficiency coaxial Ge detector sat directly above the source and at right angles to the telescope. As in the previous experiment, the tape was moved from the accumulation point to the counting position. In this case we used a symmetric cycle of 230 s collection and 230 s measurement.

The electron spectrum and the corresponding γ-ray spectrum were recorded simultaneously. Coincidences and direct spectra were recorded. The γ-ray detectors were calibrated in absolute efficiency using standard sources of ^{133}Ba and ^{152}Eu. Because the singles spectra were used for the analysis, the dead time for the electron and γ spectra was negligible. The values of the conversion coefficients are the mean values obtained from different magnet settings. The error associated with the use of the various curves in Fig. 5 was estimated by eye. The multipolarities of the transitions were then deduced from a comparison with the theoretical values [37], as shown in Fig. 6.

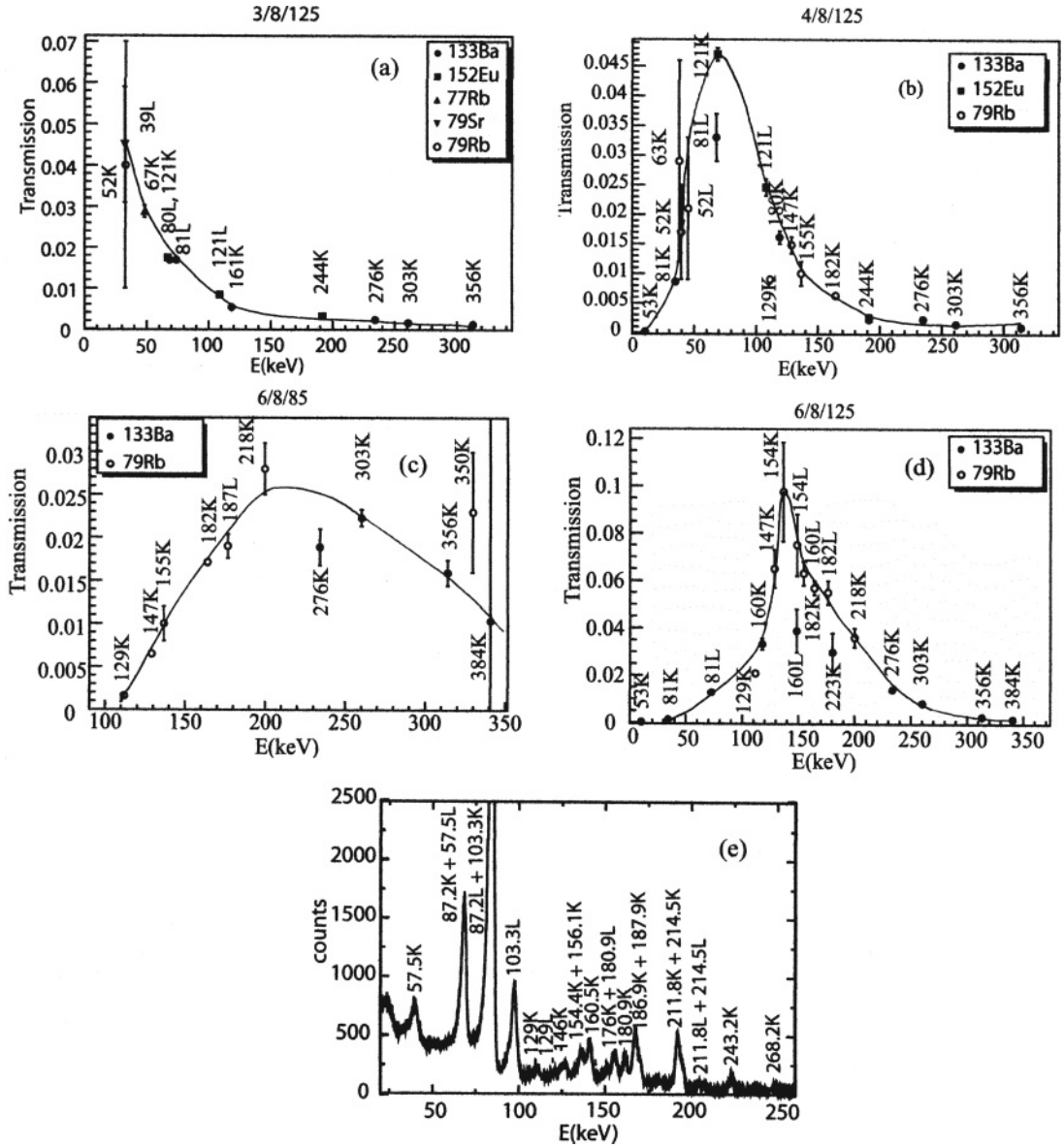

FIG. 5. The top four graphs show the measured transmission points for the four separate arrangements of the mini-orange used in the present work. They are classified by $A/B/C$ where A is the number of magnets, B is the distance from the electron source to the front face of the mini-orange, and C is the distance from the source to the Si(Li) detector (see Fig. 9 and text). Because only one type of magnet was used in the present work there is no need to specify the magnet type (see text). The measurements were made with both standard sources of ^{133}Ba and ^{152}Eu and with sources prepared *in situ* of ^{77}Rb, ^{79}Sr, and ^{79}Rb. In case of discrepancy between the transmission given by the standard and the internal sources, the latter were favored when plotting the transmission curve. This discrepancy was caused by the difficulty of placing the standard sources at precisely the same point where the transport tape places the mass-separated source for the measurement. In general, if there is a large discrepancy between the internal and the external lines this region is not used for the determination of conversion coefficients. In the bottom panel is shown a conversion electron spectrum measured with the arrangement 6/8/125. The conversion electron lines are marked with the energies of the electromagnetic transition involved and the atomic shell in which conversion occurred. All of them are assigned to transitions in ^{78}Rb. Note that the binding energies for the K-, L1-, and L2- shells are 15.2, 2.07, and 1.87 keV, respectively.

III. THE DECAY SCHEME OF ^{78}Sr

The energies, intensities, and multipolarities of the electromagnetic transitions observed in the decay of ^{78}Sr are listed in Table I together with the energies of the levels they deexcite. In general, the energies and intensities are the mean values derived from all of the singles spectra in the first experiment. Where the energies are derived from coincidence measurements they are marked with an asterisk. Summing corrections based on Monte Carlo calculations using the experimental geometry were applied where needed. The level energies were obtained using a program [38] which uses as an input all the γ rays feeding and deexciting each level and adjusts their

TABLE I. List of the γ-ray energies, relative intensities, conversion coefficients of the K and L shells when measured, multipolarities from the β decay of ^{78}Sr with their uncertainties, and the level they decay from. The intensities are normalized to that of the 103.3-keV γ ray. In general, the energies and intensities were obtained from the mean values derived from the singles spectra. The γ-ray energies and intensities obtained from coincidences have been marked with an asterisk. Those γ rays that could not be placed in the level scheme but belong to the β decay of ^{78}Sr have been underlined.

E_γ (keV)	Relative intensity	α_K	α_L	σ,λ	E_{level} (keV)	E_γ (keV)	Relative intensity	α_K	α_L	σ,λ	E_{level} (keV)
25.0(2)	720(40)				315.2	401.3(3)	570*(40)				504.7
46.9(2)	8900(300)				46.9	457.8(2)	1800*(140)				504.7
57.5(4)	483(8)		0.0846(17)	$M1$	160.8	457.9(2)	450*(40)				561.3
62.4(2)	80(14)				255.3	477.3(3)	356(12)				1038.5
75.0(3)	120(30)					504.9(2)	410(30)				504.7
87.2(5)	3030*(90)	0.21(3)		$M1$	134.0	540.0(4)	445(10)				830.1
89.7(3)	96(4)				193.0	545.8(7)	33(7)				801.6
98.3(3)	84(7)	0.55(11)		$M1/E2$	232.3	561.3(2)	1110(40)				561.3
103.1(3)	10 000(180)		0.014(2)	$M1$	103.3	575.0(2)	114(6)				830.1
112.6(9)	140(8)	0.11(5)		$E1/M1$	232.3	580.3(2)	305(12)				895.7
128.8(3)	140*(18)	0.032(11)		$E1$	232.3	613.7(4)	517(14)				
129.3(4)	110*(18)				290.2	664.0*(3)	70*(30)				895.7
133.8(2)	156(11)				134.0	698.2(2)	76(6)				801.6
140.2(2)	74(12)				274.2	722.8(2)	389(14)				826.3
146.0(4)	298(8)	0.054(12)		$M1$	193.0	726.2(2)	178(10)				830.1
154.4(4)	144(5)	0.063(18)		$M1/E2$	315.2	734.7(2)	89(6)				895.7
156.1(2)	795(15)	0.017(5)		$E1$	290.2	753.9(3)	318(18)				
160.5(4)	300(12)	0.08(2)		$M1/E2$	160.8	778.5(3)	290(17)				1283.4
170.4(3)	390(30)					792.4(2)	878(17)				895.7
180.9(3)	1980(30)	0.013(2)		$E1$	315.2	805.6(5)	210(20)				1038.5
186.9(6)	2360(30)	0.023(5)		$M1$	290.2	830.3(2)	191(9)				933.7
189.7(4)	1255(12)	0.024(9)		$M1$	504.7	845.5(3)	59(15)				1038.5
211.8(2)	4450(50)	0.020(3)	0.0027(6)	$M1$	315.2	877.8(3)	309(8)				1038.5
214.5(3)	2560(40)	0.023(8)	0.0027(7)	$M1$	504.7	895.7(2)	146(7)				895.7
243.3(2)	6490(120)				290.2	904.5(2)	52(3)				1038.5
255.3(2)	140(20)				255.3	968.1(2)	311(16)				1283.4
268.2(2)	4490(110)				315.2	1033.3(4)	69(4)				1194.1
290.1(2)	795(15)				290.2	1038.7(2)	194(10)				1038.5
325.8(2)	391(15)				830.1	1194.1(2)	141(6)				1194.1
357.8(2)	520(20)					1283.6(3)	98(7)				1283.4
370.7(2)	689(13)				504.7	1635.5(9)	64(6)				1738.9
400.5(5)	45*(15)				561.3	1660.2(5)	108(7)				1950.4

energies. Table II lists the γ rays coincident with each γ-ray transition placed in the level scheme of ^{78}Sr β decay.

The decay scheme for ^{78}Sr to levels in ^{78}Rb based on the present work is shown in Figs. 7 and 8. The normalization factor between the γ-transition intensities given in Table I and Figs. 7 and 8 is 0.3168. The level energies, the I^π values, the β feeding and the associated log ft and B(GT) values are given in Table III. The β feeding to the observed levels was deduced from the intensity balances assuming no direct feeding to the ground state and correcting the intensities of all transitions for the effect of internal conversion. The log ft values were calculated based on the log f tables derived by Gove and Martin [39]. The Q_{EC} value is taken from Ref. [41]. In what follows we discuss how we have made the spin and parity assignments to the levels in ^{78}Rb. In our work we have confirmed the 7 excited levels observed by Mukai *et al.* [24] and the 15 transitions observed by Grawel *et al.* [23]. Moreover, 10 of the levels seen in the present work were also observed in the in-beam study by Kaye *at al.* [26].

Our starting point is as follows. It seems clear that the levels at 290.2, 315.2, 504.7, and 561.3 keV all have spin and parity 1^+ because they are fed strongly in the β decay of the ^{78}Sr ground state with log ft values fully consistent with allowed Gamow-Teller character [42]. We have also adopted spin and parity 0^+ for the ^{78}Rb ground state. The spin was determined by the atomic beam resonance measurements of Ekström *et al.* [43]. Initially, positive parity was assigned because it is difficult to find any suitable configuration which gives 0^- spin and parity. Similar arguments have been advanced in earlier publications [43,44] on this topic. More convincingly, McNeill *et al.* [25] showed that the isomeric spin 4 state at 111.2 keV and the ground state have opposite parities.

TABLE II. List of observed coincident γ ray lines for each γ transition observed in the ^{78}Sr β decay. The γ-ray transitions underlined correspond to transitions which belong to the ^{78}Sr β decay but have not been placed in the level scheme. The coincident γ-ray lines that correspond to ^{78}Rb β decay have been marked with a double asterisk.

E_γ(keV)	Coincident lines
25.2	46.9, 57.5, 87.2, 103.1, 129.3, 133.8, 156.1, 160.5, 170.4, 186.9, 189.7, 243.3, 290.1, 325.8, 580.3, 753.9, 778.5, 968.1
46.9	Rb-*x*, 25.0, 62.4, 87.2, 98.3, 140.2, 146.0, 156.1, 180.9, 189.7, 214.5, 243.3, 268.2, 325.8, 370.7, 457.8, 540.0, 545.8, 575.0, 580.3, 664.0, 753.9, 778.5, 845.5, 904.5, 968.1, 1660.2
57.5	Rb-*x*, 25.0, 103.1, 129.3, 154.4, 189.7, 214.5, 325.8, 400.5, 477.3, 540.0, 580.3, 613.7, 734.7, 778.5, 877.8, 968.1, 1033.3, 1660.2
62.4	Rb-*x*, 46.9, 89.7, 103.1, 146.0, 545.8, 575.0
75.0	Rb-*x*, 211.8
87.2	Rb-*x*, Kr-*x*, 25.0, 46.9, 98.3, 140.2, 156.1, 180.9, 189.7, 214.5, 325.8, 370.7, 540.0, 580.3, 664.0, 693.0**, 778.5, 805.6, 904.5, 968.1, 1660.2
89.7	Rb-*x*, 62.4, 103.1, 545.8, 575.0, 845.5
98.3	Rb-*x*, 46.9, 87.2, 133.8, 664.0, 805.6
103.1	Rb-*x*, 25.0, 57.5, 62.4, 89.7, 128.8, 129.3, 154.4, 186.9, 189.7, 211.8, 214.5, 325.8, 400.5, 401.3, 457.9, 477.3, 540.0, 545.8, 575.0, 580.3, 664.0, 698.2, 722.8, 726.2, 734.7, 778.5, 792.4, 805.6, 830.3, 845.5, 877.8, 968.1, 1033.3, 1635.5, 1660.2
112.6	Rb-*x*, 664.0, 805.6
128.8	Rb-*x*, 103.1, 664.0, 805.6
129.3	Rb-*x*, 25.0, 57.5, 103.1, 160.5, 189.7, 214.5, 325.8, 540.0, 580.3, 778.5, 968.1, 1660.2
133.8	Rb-*x*, 25.0, 98.3, 140.2, 156.1, 180.9, 189.7, 214.5, 325.8, 370.7, 540.0, 580.3, 664.0, 778.5, 805.6, 904.5, 968.1, 1660.2
140.2	Rb-*x*, 46.9, 87.2, 133.8
146.0	Rb-*x*, 46.9, 62.4, 545.8, 575.0, 845.5
154.4	Rb-*x*, 57.5, 103.1, 160.5, 189.7, 325.8, 357.8, 580.3, 778.5, 968.1
156.1	Rb-*x*, 25.0, 46.9, 87.2, 133.8, 189.7, 214.5, 325.8, 540.0, 580.3, 778.5, 968.1, 1660.2
160.5	Rb-*x*, 25.0, 129.3, 154.4, 189.7, 214.5, 325.8, 400.5, 477.3, 540.0, 580.3, 734.7, 778.5, 877.2, 968.1, 1033.3, 1660.2
170.4	Rb-*x*, 25.2, 214.5, 540.0, 805.6
180.9	Rb-*x*, 46.9, 87.2, 133.8, 189.7, 325.8, 580.3, 778.5, 968,1
186.9	Rb-*x*, 25.0, 103.1, 189.7, 214.5, 325.8, 540.0, 580.3, 613.8, 778.5, 968.1, 1660.2
189.7	Rb-*x*, 25.0, 46.9, 57.5, 87.2, 103.1, 129.3, 133.8, 154.4, 156.1, 160.5, 180.9, 186.9, 211.8, 243.3, 268.2, 290.1, 325.8, 778.5
211.8	Rb-*x*, 75.0, 103.1, 189.7, 325.8, 580.3, 613.7, 778.5, 968.1
214.5	Rb-*x*, 46.9, 57.5, 87.2, 103.1, 129.3, 133.8, 156.1, 160.5, 170.4, 186.9, 243.3, 290.1, 325.8, 613.7, 753.9, 778.5
243.3	Rb-*x*, 25.0, 46.9, 189.7, 214.5, 325.8, 540.0, 580.3, 778.5, 968.1, 1660.2
255.3	Rb-*x*, 545.8, 575.0
268.2	Rb-*x*, 46.9, 189.7, 325.8, 580.3, 778.5, 968.1
290.1	Rb-*x*, 25.0, 189.7, 214.5, 290.1, 540.0, 580.3, 778.5, 968.1, 1660.2
325.8	Rb-*x*, 25.0, 46.9, 57.5, 87.2, 103.1, 129.3, 133.8, 154.4, 156.1, 160.5, 180.9, 186.9, 189.7, 211.8, 214.5, 243.3, 268.2, 290.1, 370.7, 401.3, 457.8, 504.9
357.8	Rb-*x*, 154.4, 561.3, 805.6
370.7	Rb-*x*, 46.9, 87.2, 133.8, 325.8, 778.5
400.5	Rb-*x*, 57.5, 103.1, 160.5, 477.3
401.3	Rb-*x*, 103.1, 325.8, 778.5
457.8	Rb-*x*, 46.9, 325.8, 778.5
457.9	Rb-*x*, 103.1, 477.3
477.3	Rb-*x*, 57.5, 103.1, 160.5, 400.5, 457.9, 561.3
504.9	Rb-*x*, 325.8, 778.5
540.0	Rb-*x*, 46.9, 57.5, 87.2, 103.1, 129.3, 133.8, 156.1, 160.5, 170.4, 186.9, 243.3, 290.1
545.8	Rb-*x*, 46.9, 62.4, 89.7, 103.1, 146.0, 255.3
561.3	Rb-*x*, 477.3, 357.8
575.0	Rb-*x*, 46.9, 62.4, 89.7, 103.1, 146.0, 255.3
580.3	Rb-*x*, 25.0, 46.9, 57.5, 87.2, 103.1, 129.3, 133.8, 154.4, 156.1, 160.5, 180.9, 186.9, 211.8, 243.3, 268.2, 290.1
613.7	Rb-*x*, 57.5, 186.9, 211.8, 214.5
664.0	Rb-*x*, Kr-*x*, 46.9, 87.2, 98.3, 103.1, 112.6, 128.8, 133.8, 455.0
698.2	Rb-*x*, 103.1
722.8	Rb-*x*, 103.1
726.2	Rb-*x*, 103.1
734.7	Rb-*x*, 57.5, 103.1, 160.5

TABLE II. (*Continued*)

E_γ(keV)	Coincident lines
753.9	Rb-x, 25.2, 46.9, 214.5
778.5	Rb-x, 25.0, 46.9, 57.5, 87.2, 103.1, 129.3, 133.8, 154.4, 156.1, 160.5, 180.9, 186.9, 189.7, 211.8, 214.5, 243.3, 268.2, 290.1, 370.7, 401.3, 457.8, 504.9
792.4	Rb-x, 103.1
805.6	Rb-x, 87.2, 98.3, 103.1, 112.6, 128.8, 133.8, 170.4, 357.8
830.3	Rb-x, 103.1
845.5	Rb-x, 46.9, 89.7, 103.1, 146.0
877.8	Rb-x, 57.5, 103.1, 160.5
904.5	Rb-x, 46.9, 87.2, 133.8
968.1	Rb-x, 25.0, 46.9, 57.5, 87.2, 103.1, 129.3, 133.8, 154.4, 156.1, 160.5, 180.9, 186.9, 211.8, 243.3, 268.2, 290.1
1033.3	Rb-x, 57.5, 103.1, 160.5
1038.7	Rb-x
1194.1	Rb-x
1283.6	Rb-x
1635.5	Rb-x, 103.1
1660.2	Rb-x, 46.9, 57.5, 87.2, 103.1, 129.3, 133.8, 156.1, 160.5, 186.9, 243.3, 290.1

Earlier, Ekström *et al.* [43] had shown that the measured magnetic moment of the isomeric state is in close agreement with the theoretical value for the $\pi[422]5/2^+ - \nu[301]3/2^-$ configuration. In other words, it is of negative parity. No available configuration of positive parity can reproduce the large measured value of the magnetic moment for the isomeric level. Thus, we believe that the I^π of the isomeric state is 4^- and consequently the parity of the ground state is positive. Although the measurements reported here were not sensitive to any ground-state-to-ground-state feeding, the total absorption studies of the same decay [45] showed that there is little or no such feeding. This is what one would expect for an isospin-forbidden 0^+ to 0^+ β decay.

TABLE III. Measured β-decay feedings and the log ft and B(GT) values obtained for each energy level. The latter have been calculated using the expression $B(\mathrm{GT}) = K \times \frac{1}{ft}$, with f the value of the Fermi function for $(Q_{\mathrm{EC}} - E)$, t the partial half-life, and $K = 3809.0(10)$ [40]. The I^π values for the energy levels are also listed.

E_{level} (keV)	I^π	β_{feeding} (%)	log ft	B(GT) ($\times 10^2$)
0	0^+	0		
46.9	1^-	0(2)	8(2)	0.004(18)
103.3	1^+	1.6(7)	6.14(19)	0.28(12)
119.6	(3^+)			
134.0	1^-	0.1(4)	7.3(18)	0.02(8)
160.8	1^+	1.15(11)	6.18(5)	0.25(3)
193.0	0^-,1^-,2^-	0.81(9)	6.37(6)	0.16(2)
232.3	$(2)^-$	0.46(14)	7.91(14)	0.0047(15)
255.3	1^+,1^-,2^+	0.32(10)	6.73(14)	0.07(2)
274.2	2^-	0.24(4)	8.15(8)	0.0027(5)
290.2	1^+	3.8(12)	5.63(14)	0.9(3)
315.2	1^+	49.1(12)	4.50(2)	12.0(5)
504.7	1^+	21.0(5)	4.72(2)	7.3(3)
561.3	1^+	3.92(19)	5.41(3)	1.48(10)
801.6		0.35(3)	6.26(4)	0.21(2)
826.3	1^+	1.22(5)	5.70(3)	0.76(5)
830.1	1^+	3.55(7)	5.23(2)	2.24(9)
895.7	1^+	4.67(12)	5.05(2)	3.39(15)
933.7	1^+	0.60(3)	5.91(3)	0.47(3)
1038.5	1^+	3.72(10)	5.02(2)	3.64(17)
1194.1	1^+	0.66(2)	5.62(2)	0.91(5)
1283.4	1^+	2.20(7)	5.02(2)	3.64(19)
1738.9	1^+	0.20(2)	5.62(5)	0.91(11)
1950.4	1^+	0.33(2)	5.21(3)	2.35(19)

With the above in mind we now review the I^π assignments we have made to the levels in ^{78}Rb.

46.9-keV level. This level is fed by an $M1$ transition of energy 87.2 keV (see Fig. 7) deexciting the 134.0-keV level, which has a firm assignment of 1^- (see the later discussion of this level), and decays to the ground state. It is thus firmly established as $I^\pi = 1^-$. This is in accord with the reported measurements of McNeill *et al.* [25], where the 46.9-keV transition was determined to have $E1$ multipolarity. The lifetime of this level has been measured by Mukai *et al.* [24] as 910(40) ns and by Kaye *et al.* [26] as 610(100) ns. In broad terms the transition rates obtained from these lifetimes are consistent with electric dipole multipolarity in the region [42]. In the case of Kaye *et al.* the value was cross-checked with a measurement they made of the lifetime of the 66.5-keV level in ^{77}Kr.

103.3-keV level. As shown in Fig. 7 the 103.3-keV level decays by an $M1$ transition to the ground state. This establishes its spin and parity as 1^+. It is fed by $M1$ transitions with energies 186.9 and 211.8 keV from 1^+ levels, which agrees with this assignment.

111.2-keV level. This isomeric level is not populated in the ^{78}Sr β decay and is included here and in Fig. 7 for the sake of completeness. As mentioned earlier, 4^- is the most reasonable choice for the spin and parity of this level in view of the results of Ekström *et al.* [43] and McNeill *et al.* [25].

119.6-keV level. Kaye *et al.* report a level at this energy, which decays by an unseen low-energy transition. Our results are consistent with its existence through the observation of

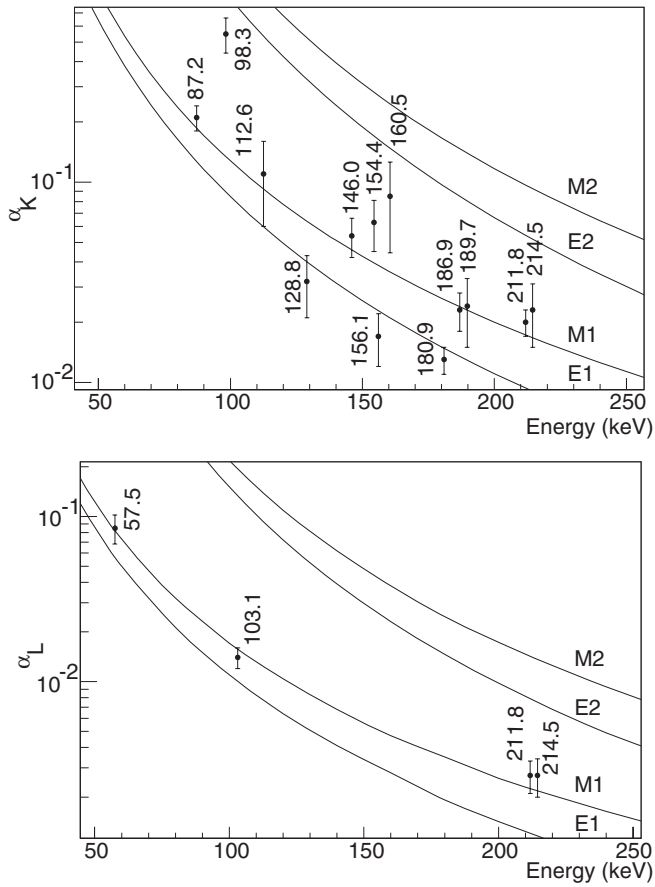

FIG. 6. The measured conversion coefficients for transitions in ^{78}Rb measured in studies of the decay of ^{78}Sr. The top graph shows the K component of the conversion coefficients and the lower one the L- or the $L + M$ component if they cannot be resolved. The points are labeled with the shell in which conversion occurs and the energy of the transition.

coincidences between the 112.6-keV and the 664.0- and 805.6-keV transitions. This level is fed by an $E1$ or an $M1$ 112.6-keV transition from a level at 232.3 keV, which we believe is a $(2)^-$ (see below). A 170.4-keV line observed in coincidence with the 25.2-, 214.5-, and 540.0-keV γ-ray lines could possibly feed this level from the 290.0-keV level. However, the coincidence of this 170.4-keV line with the 805.6-keV γ ray is in disagreement with its suggested placement and no firm conclusions have been drawn. A possible explanation would be the existence of a doublet at an energy of 170 keV, which would solve this inconsistency. No de-exciting transitions were observed from this level to either the 0^+ ground state or the 1^- level at 46.9 keV. It is likely that the de-excitation proceeds through a highly converted transition to one of the other lower-lying levels. The planar detector threshold in our case is too low to observe a transition of 8.4 keV to the 111.2-keV level. A 16.8-keV $E2$, if it exists, is below our sensitivity. This explains why there is no value for this level in Fig. 7.

134.0-keV level. This level is fed by the 156.1-keV $E1$ transition from the 1^+ level at 290.2 keV. It decays to the ground state, which establishes it as a 1^- state. As mentioned above, the $M1$ character of the transition of 87.2 keV to the 46.9-keV level fixes that state as a 1^- state. The level at 134.0 keV was seen in the heavy-ion fusion evaporation study by Kaye *et al*. [26]. They assign spin and parity 2^- on the basis of the measured directional correlations de-exciting oriented states (DCO) ratios for the 87.2-keV transition. The reported DCO ratios appear to be consistent with either $E1$ or $M1$ multipolarity, which is consistent with our $M1$ assignment from the K conversion coefficient. Not surprisingly, they did not see the 133.8-keV transition to the ground state because it appears to be below their sensitivity limit. We believe that the correct I^π is 1^- and this has the consequence that the levels in both band 5 and band 6 in their paper would have spins lower by one unit.

160.8-keV level. The 160.5-keV transition to the ground state has a multipolarity of mixed $M1/E2$ character. This fixes the I^π of the 160.8-keV level as 1^+. This is corroborated by the fact that it is fed by an $M1/E2$ transition from the 1^+ level at 315.2 keV. We have determined that the 57.5-keV de-exciting transition to the 103.3-keV level is of $M1$ character. It should be noted that our assignments are in disagreement with those of Kaye *et al*. [26], who, on the basis of DCO ratio measurements in a heavy-ion, fusion-evaporation reaction study, assign $E2$ and stretched $M1$ character to the 160.5- and 57.5-keV transitions, respectively. Our assignment would lower the spin of their band 9 by one unit.

193.0-keV level. This level decays by an $M1$ transition of 146.0 keV to a 1^- level. This makes it of negative parity with a spin of 0, 1, or 2. This is consistent with the small amount of feeding in the β decay (see below).

232.3-keV level. This level was observed in beam by Kaye *et al*. [26]. Although we also observe three deexciting transitions of roughly the same energies the branching ratio they report for the 129.2-keV transition is clearly inconsistent with our observations. Instead, we see a much weaker 128.8-keV transition deexciting this level. The fact that we see another 129.3-keV transition deexciting the 290.2-keV level, a level not observed by Kaye *et al*., does not resolve this inconsistency. Here we observe an $M1/E2$ transition of 98.3 keV to a firm 1^- state and an $E1$ transition of 128.8-keV transition to a firm 1^+ state. This fixes negative parity and allows spins 0, 1, or 2. The 1^- assignment is unlikely because we do not see the transition to the ground state. However, considering the earlier discussion in relation to the 119.6-keV level, 2^- is clearly favored.

255.3-keV level. The 255.3-keV level decays to the ground state and to the 193.0-keV level. Thus, it can have $I^\pi = 1^-$, 1^+, or 2^+. The reader may object to the fact that we have not ruled out the 2^+ and 2^- assignments to the 255.3- and 193.0-keV levels on the basis of the relatively large log ft values, which would agree with first forbidden transitions, but not with second forbidden transitions (as would be the case for spins and parities 2^+ and 2^-). However, in these two cases the feeding, based on the intensity balance into and out of the levels, is only 0.3% and 1.0%, respectively. These values are low enough that they could be attributed to indirect feeding by unobserved transitions from higher-lying levels. This is a manifestation of the so-called *pandemonium* effect [46].

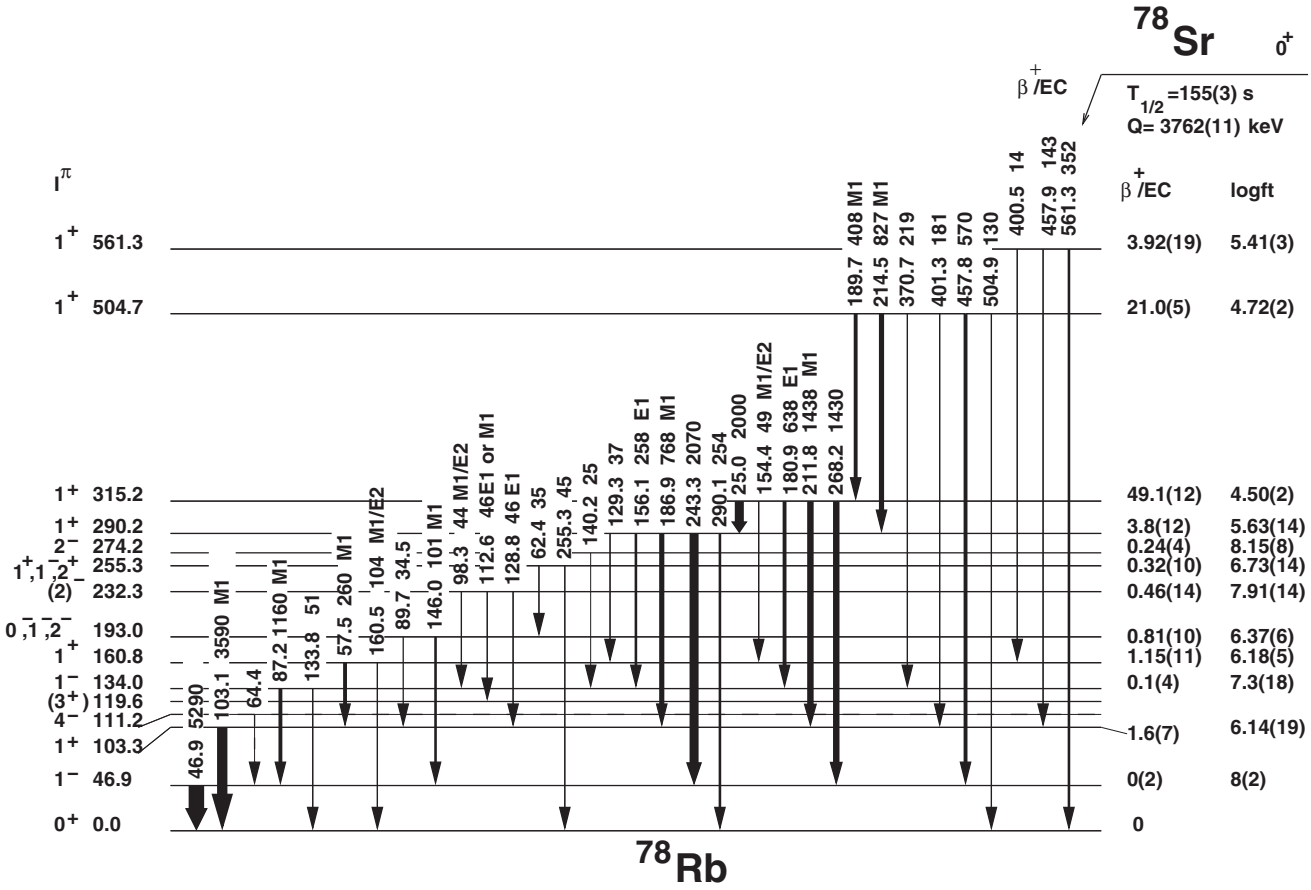

FIG. 7. Here we see part of the decay scheme for ^{78}Sr deduced in the present work. The assigned I^{π} values and level energies in keV are shown on the left. The percentage feeding in the β decay and corresponding log ft values are shown on the right. The γ-ray energies and multipolarities measured in the present work are marked on the figure. It should be noted that the transition intensities are normalized to a total intensity of 10 000 units feeding the ground state. The ^{78}Sr half-life and the Q_{EC} [41] are also shown. For completeness the isomeric level at 111.2 keV and the 64.4-keV deexciting transition (dashed line) [25] are included, although the level is not populated in the decay. Note that McNeill *et al.* [25] observed the conversion electrons from the 46.9- and 64.4-keV transitions. They assigned multipolarities of $M1$ and $M3$ character to the two transitions. This establishes the fact that the 111.2-keV level and the ground state have different parities.

274.2 keV. A level at this energy is populated strongly in the in-beam studies of Kaye *et al.* [26]. In their work and based on DCO ratios, they see a 140-keV stretched $M1$ transition to the 134-keV level, which they assigned as a 2^- level. From our data we deduce that the 134-keV level has spin and parity 1^- and using their information we assign 2^- to the 274.2-keV level.

290.2-, 315.2-, 504.7-, and 561.3-keV levels. We remind the reader that at the beginning of this discussion we assumed that all of these levels have $I^{\pi} = 1^+$ based on the log ft values. Nothing in the decay scheme we have constructed contradicts this assumption. It should be noted that Kaye *et al.* [26] also report the levels at 290.2 and 504.7 keV, with the latter decaying to the former. Two of the deexciting transitions from the 290.2 keV level observed by us were not seen and the 214.5-keV transition was the only line seen from the 504.7-keV level. We would judge that the other transitions were not seen because they are below the level of sensitivity in their experiment. The branching ratios they report for the 290.1-keV level are in poor agreement with those reported here. Kaye *et al.* also report the 315.2-keV level as decaying via the 211.8- and 180.9-keV transitions but do not see the other transitions reported here. Because the 268.2-keV transition has an intensity comparable to the 211.8-keV transition this is surprising. They assign $I^{\pi} = (2^+)$ to this level, which is ruled out by the small log ft value.

Levels above 600 keV. All of these levels have log ft values less than 5.9. Consequently, based on the compilation of Raman and Gove [47] of log ft values for allowed Gamow-Teller transitions, they are all assigned as 1^+ states. This assignment is in accord with all the transitions deexciting these levels to the levels discussed above.

Finally, it is worth noting that the levels observed by us and discussed in this section up to 505 keV energy were also seen in the in-beam experiment reported by Kaye *et al.* [26] with the exception of the levels at 193.0 and 255.3 keV.

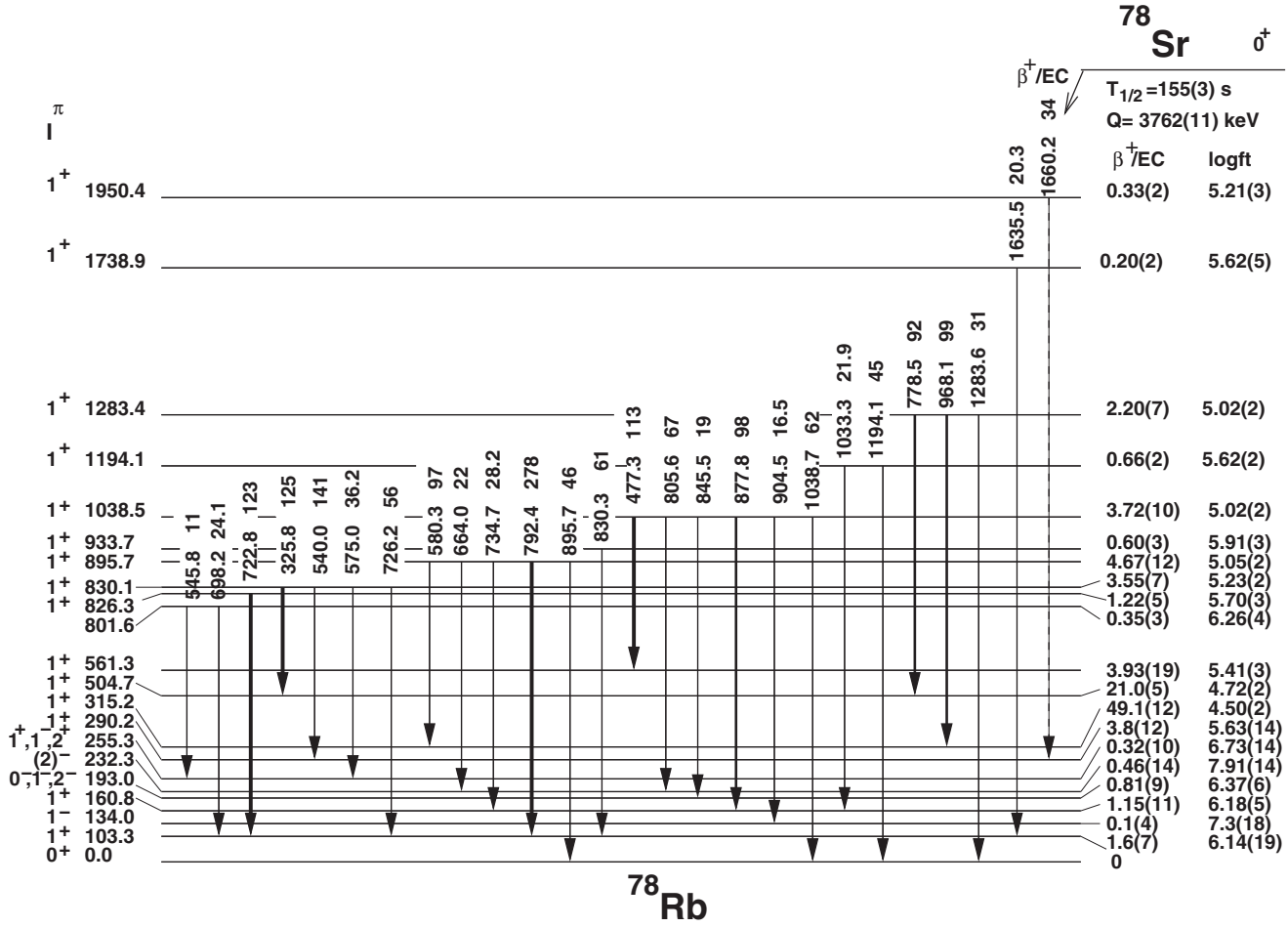

FIG. 8. Same as for Fig. 7 but now including levels above 600 keV. Note that the levels at 46.9, 111.2, 119.6, and 274.2 keV have been omitted because we do not see transitions feeding them from higher levels.

IV. DISCUSSION

We now discuss the structure of the levels in ^{78}Rb observed in the present experiment. We include in our discussion the 4^- isomeric level because its properties are germane to the discussion although it is not populated in this decay. We restrict ourselves to the levels in Fig. 7, the lower part of the level scheme, because at higher energies the levels are probably too mixed to allow us any clear-cut interpretation.

It is convenient for this purpose to group the levels into four "families" or categories, which we will discuss in turn. The first of these, family A, consists of the four 1^+ levels that have small log ft values. They lie at 290.2, 315.2, 504.7, and 561.3 keV in excitation energy. Family B are the observed negative parity states at 46.9 (1^-), 134.0 (1^-), 193.0 (0^-,1^-,2^-), 232.3 (2^-), and 274.2 (2^-). The 255.3-keV (1^+,1^-,2^+) level and the 4^- isomeric state at 111.2 keV are also included in family B (see below). Family C has the two 1^+ levels with very small β strength at 103.3 and 160.8 keV. Finally, we treat the ground state as being of a separate family D. Note that our present knowledge of the 119.6-keV level does not allow us to place it in any of these families.

The starting point for our understanding of the structure of ^{78}Rb lies in the nature of the ^{78}Sr ground state. This is because the deformation of the parent state can be related to the states populated in the daughter nucleus, as discussed in several papers [12,13].

A number of measurements are relevant here. First, Lister *et al.* [48] have measured the $B(E2; 2^+ \rightarrow 0^+)$ for the ground-state band in ^{78}Sr and from this they derived $Q_0(2^+) = 3.29(19)$ b. This is consistent with the prediction of Möller and Nix [49] of $Q_0 = +3.2$ b. Lister *et al.* [2] also pointed out that this large prolate deformation is supported by the quadrupole moment they extract for ^{79}Sr from the ground-state band in that nucleus. The isotope shift measurements of Buchinger *et al.* [50] support a large $\delta\langle r\rangle^2$ for ^{78}Sr from which one can derive a large deformation of $\sqrt{\beta}^2 \simeq 0.38$. All of this information is consistent with a large deformation.

Calculations of the β feeding to the states in ^{78}Rb from the ^{78}Sr ground state have been published in Ref. [28]. In those calculations a quasiparticle basis is first constructed self-consistently from a deformed Hartree-Fock (HF) calculation with density-dependent Skyrme forces and pairing correlations in the BCS framework. The minima in a plot of the total HF energy versus deformation give the possible deformations of the ground state. For ^{78}Sr two minima are found, one prolate with $\beta = 0.42$ and the other spherical. Finally, a

TABLE IV. Two-quasiparticle excitation energies and their associated asymptotic numbers $[Nn_z\Lambda]\Omega^\pi$ (spherical shells) in ^{78}Rb for prolate (spherical) shapes. Also shown are the spins resulting from the Gallagher-Moszkowski coupling rules, as well as the spins obtained from the opposite sense of the rules (within parentheses). The results correspond to Skyrme HF + BCS calculations with the Skyrme force SG2.

E_x (MeV)	Prolate Nilsson configuration	Spin	E_x (MeV)	Spherical Spherical shell	Spin
0.76	$\pi[431]3/2^+\ \nu[431]1/2^+$	$1^+(2^+)$	0.79	$\pi p_{3/2} - \nu p_{1/2}$	$1^+(2^+)$
0.74	$\pi[312]3/2^-\ \nu[301]3/2^-$	$0^+(3^+)$			
0.57	$\pi[312]3/2^-\ \nu[422]5/2^+$	$1^-(4^-)$			
0.33	$\pi[422]5/2^+\ \nu[301]3/2^-$	$4^-(1^-)$	0.44	$\pi f_{5/2} - \nu p_{1/2}$	$3^+(2^+)$
0.17	$\pi[431]3/2^+\ \nu[301]3/2^-$	$3^-(0^-)$			
0.16	$\pi[422]5/2^+\ \nu[422]5/2^+$	$5^+(0^+)$			
0.0	$\pi[431]3/2^+\ \nu[422]5/2^+$	$4^+(1^+)$	0.0	$\pi p_{1/2} - \nu p_{1/2}$	$1^+(0^+)$

separable spin-isospin residual interaction is introduced in both particle-hole and particle-particle channels and treated in the quasiparticle random phase approximation (QRPA). In calculating the B(GT) values it is also assumed that the parent state and the states populated have the same deformation. The quasiparticle orbitals in the vicinity of the Fermi level predicted by our Skyrme (SG2) HF + BCS calculations are given by $[422]5/2^+$, $[431]3/2^+$, and $[312]3/2^-$ in the case of proton states and $[431]1/2^+$, $[301]3/2^-$, $[422]5/2^+$, and $[431]3/2^+$ in the case of neutron states, where $[Nn_z\Lambda]\Omega^\pi$ stands for the asymptotic quantum numbers. These states are consistent with measurements from Rb isotope shifts by Thibault *et al.* [51] that established $\pi[312]3/2^-$ and $\pi[422]5/2^+$ as the ground states of the odd-proton nuclei ^{77}Rb and ^{79}Rb, respectively. In addition, the state $\pi[312]3/2^-$ is known to be only 39 keV apart from the ground state for the latter nucleus [52]. The proton orbital $\pi[431]3/2^+$ is also proposed to be nearby. Overall, the proton orbitals expected close to the Fermi level are $\pi[312]3/2^-$, $\pi[422]5/2^+$, and $\pi[431]3/2^+$, in accord with our HF + BCS calculations. Similarly, hyperfine structure and magnetic moment measurements for a number of Kr and Sr isotopes [53], place the ordering of neutron orbitals as $[301]3/2^-$ and $[422]5/2^+$, which are also consistent with our HF + BCS calculations.

Table IV shows the low-energy proton-neutron two-quasiparticle configurations in the odd-odd daughter nucleus ^{78}Rb. We have considered the possible odd-odd configurations according to the Gallagher-Moszkowski (G-M) rules for deformed nuclei [54], that is, assuming that the lowest energy level corresponds to the case where the components Σ_p and Σ_n of the proton and neutron spin along the nuclear symmetry axis couple parallel and therefore the total spin of the odd-odd nuclear level is given by $I = \Omega_p + \Omega_n$ if $\Omega_p = \Lambda_p \pm 1/2$ and $\Omega_n = \Lambda_n \pm 1/2$ and by $I = |\Omega_p - \Omega_n|$ if $\Omega_p = \Lambda_p \pm 1/2$ and $\Omega_n = \Lambda_n \mp 1/2$. Similarly, in the spherical case, the rules are such that the lowest level in energy has $I = j_p + j_n$ if $j_p = \ell_p \pm 1/2$ and $j_n = \ell_n \pm 1/2$ and $I = |j_p - j_n|$ if $j_p = \ell_p \pm 1/2$ and $j_n = \ell_n \mp 1/2$. Thus, for each two-quasiparticle configuration we show in Table IV the spin of the lower energy state corresponding to the G-M rule. We also show within parentheses the spin corresponding to the antiparallel spin coupling, which is expected somewhat higher in energy.

The results in Table IV correspond to the force SG2, which has proved to be very successful in describing spin-isospin nuclear properties. Results for other Skyrme forces are qualitatively similar to these although they may differ in the details. We should also mention that although the B(GT) strengths are calculated at the end within QRPA, it is worth analyzing the present decay scheme with this simple and intuitive approach, which allows us to get a straightforward interpretation of the underlying excitation mechanism. Although we consider that ^{78}Sr is prolate, we use these calculations to identify spherical states in the daughter nucleus as well because they can be fed in our experiment via higher excited states or from small admixtures of spherical configurations in the parent ground state.

We first examine family B. Table IV indicates that only the prolate calculation predicts the existence of negative parity states at low energy. The coupling of $\pi[422]5/2^+$ and $\nu[301]3/2^-$ gives us a 4^- state according to the calculations and the G-M rule and a state 1^- at a higher energy. The isomeric state at 111.2 keV has been previously interpreted as the 4^- level of this configuration based on an atomic beam magnetic resonance experiment by Ekström *et al.* [43]. The observed large positive moment $\mu = 2.56\ \mu_N$ could only be reproduced by assuming a large $\pi[422]5/2^+ - \nu[301]3/2^-$ component in its wave function. This relies on a large prolate deformation which was confirmed in the isotope shift measurements of Thibault *et al.* [51]. As seen in Table IV, such a prolate deformed state of $I^\pi = 4^-$ can be accommodated in the calculations at low energy, where one level with $I^\pi = 4^-$ and the same configuration as proposed by Ekström *et al.* [43] is found (note that the alternative $\pi[312]3/2^- - \nu[422]5/2^-$ assignment for this state would result in $\mu = 0.488\ \mu_N$). We can identify the 1^- states at 46.9 and 134.0 keV with the predicted 1^- states with configurations $\pi[312]3/2^- - \nu[422]5/2^+$ and $\pi[422]5/2^+ - \nu[301]3/2^-$. The latter is the partner of the 4^- state and lies at higher excitation energy as expected. The 193.0-, 232.3-, and 274.2-keV levels also belong to this family. The fact that the 193.0-keV level was not observed in beam and the other two were favors a 0^- assignment to this level and 2^- to the 232.2- and 274.2-keV levels. We also place the 255.3-keV level into this family. Because it was not observed in beam a 2^+ assignment is not favored. The fact that it decays into the 193.0-keV level via an $E1$ transition instead of decaying via an $M1$ into 1^+ states of family C favors a 1^- assignment and prolate character. The 0^- state could arise from the $\pi[431]3/2^+ - \nu[301]3/2^-$ configuration or from $\pi[312]3/2^- - \nu[431]3/2^+$, not shown

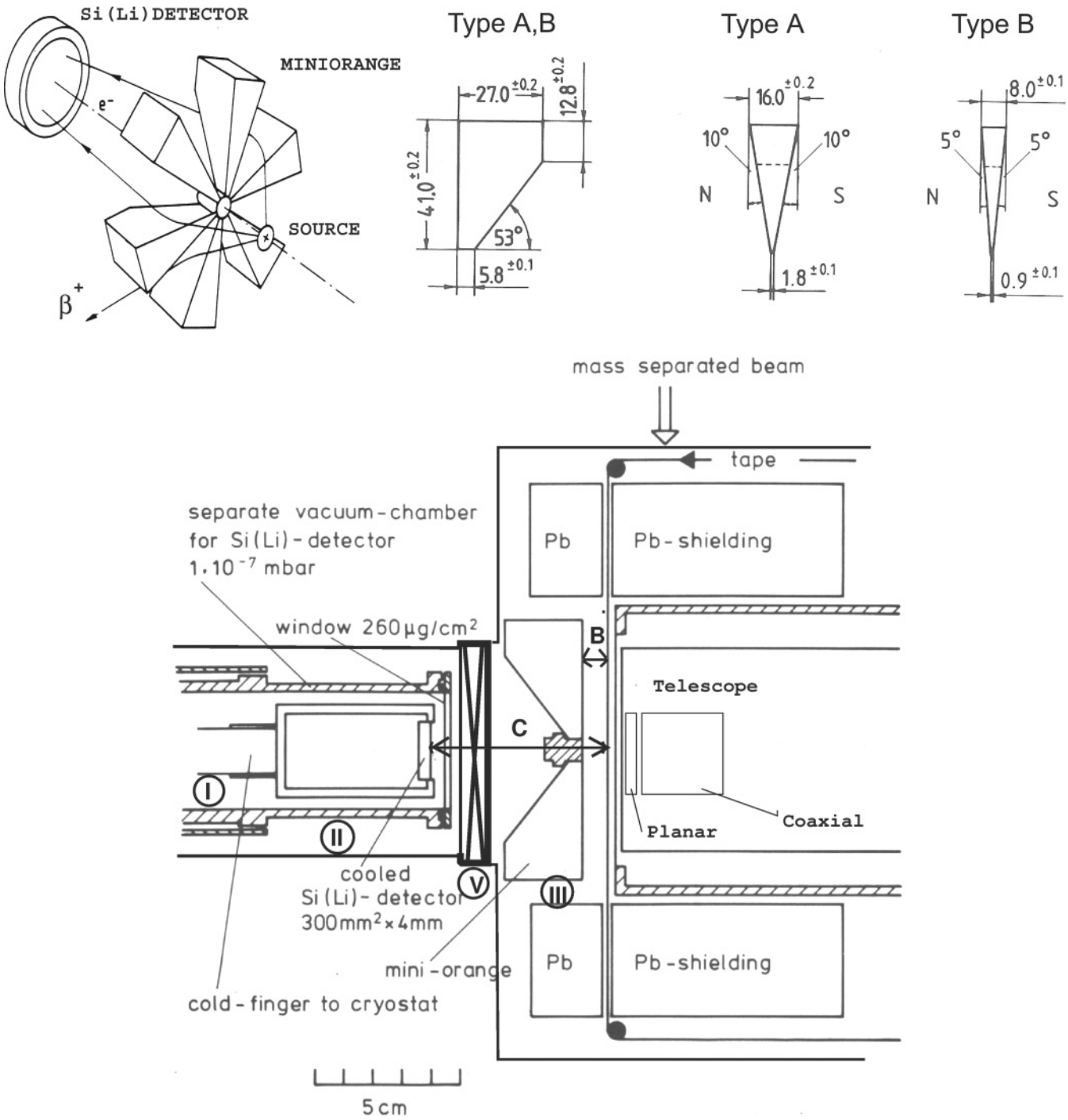

FIG. 9. A sketch of a horizontal cross section through the experimental setup for the conversion electron studies with the mini-orange spectrometer [33]. The mass-separated beam is deposited onto a tape, which is moved periodically to place the accumulated activity in front of the mini-orange and the Ge telescope (see text). These two detectors sat at 180° to one another with the source in between as shown. A coaxial Ge detector was positioned above the source at right angles to the telescope and is not shown in the figure. The distances B and C are the distances from the source to the front face of the mini-orange and the Si(Li) detector, respectively. This nomenclature is used to classify the various mini-orange setups used in the experiments as can be seen in Fig. 5 and the text. The various independent volumes in the apparatus (see text) are marked I, II, and III, respectively. There is a valve between I and II that is not shown in the figure and a valve marked V that is used to isolate II from III, the main mini-orange chamber.

in Table IV because it appears at higher energy. The 2^- states could arise from $\pi[312]3/2^- - \nu[431]1/2^+$, which also appears at higher energy, or as a member of the rotational band built on 0^- or 1^- bandheads.

Based on the small observed β feeding we conclude that the states at 103.3 and 160.8 keV have a rather different shape from the ^{78}Sr ground state and must therefore be spherical. If we look at Table IV we see that two 1^+ states of spherical shape are predicted at low energy and we therefore interpret these two observed states as the $\pi p_{1/2} - \nu p_{1/2}$ and $\pi p_{3/2} - \nu p_{1/2}$ configurations.

Turning now to the 0^+ ground state we find that Thibault *et al.* [51] also measured the isotope shift for this state. They conclude that it has a large prolate deformation. The 0^+ ground state and the observed 3^+ excited state at 119.6 keV can be interpreted as arising from the $\pi[312]3/2^-$ and $\nu[301]3/2^-$ coupling. A different possibility for the 0^+ ground state that should be considered corresponds to the $\pi[422]5/2^+$ and $\nu[422]5/2^+$ coupling. Although the G-M rule predicts in this case a 5^+ state below the 0^+ state, a violation of the G-M rule cannot be discounted. This interpretation would agree with the expectation based on the assigned ^{79}Rb ground-state configuration of $\pi[422]5/2^+$ and the $\nu[422]5/2^+$ configuration for the ^{77}Kr ground state as proposed by Ekström *et al.* [43]. One should also note that the 0^+ deformed ground state will generate a rotational band with an odd-even Newby shift in the rotational energy levels.

The main characteristic of the 1^+ states in family A is the small log ft values which link them closely to the ^{78}Sr parent state structure. Thus, we see them as prolate-deformed states. From Table IV we see that two prolate states are predicted at low excitation energy with configurations $\pi[431]3/2^+ - \nu[422]5/2^+$ and $\pi[431]3/2^+ - \nu[431]1/2^+$ and can therefore be assigned as possible configurations for the two lowest states. In the first case a 4^+ state is expected below the 290.0-keV 1^+ level, which could be identified with the 4^+ level observed at 115 keV energy in the in-beam experiments [26].

V. SUMMARY

We have studied the β^+/EC decay of ^{78}Sr. We have carried out measurements of the energies and intensities of the emitted γ rays and conversion electrons as well as γ-γ and γ-x-ray coincidences, which have extended our knowledge of the decay scheme of ^{78}Sr including spin and parity assignments to the levels populated in the daughter nucleus ^{78}Rb. The very much improved experimental knowledge of the ^{78}Rb levels populated in the decay and the strong link between the parent and the daughter states allowed us to infer some possible level configurations. Measurements with a TAS spectrometer will be reported in a separate publication. The structure of odd-odd nuclei is, in general, difficult to interpret and even more so in this part of the nuclear chart, where shape coexistence is common. Although a simple calculation based on a mean-field approach does not always permit us to associate an observed excited state with a definite configuration, we believe that the results of the β decay study and the comparison with calculations allow us to make a more advanced interpretation than has been usual for the difficult case of odd-odd nuclei.

ACKNOWLEDGMENTS

This work was supported in part by the Spanish MEC under Grant No. FPA2005-03993 and a Formacion Profesorado Universitario (FPU) fellowship (FPA2003-4041). It was also supported by MICINN nuclear Grants No. FPA2008-06419-C02-01, No. FPA2009-07387, and No. FPA2010-17142 and by the U.K. Science and Technology Facilities Council (STFC) Grant No. ST/F012012/1. The experiments were partly supported through EURONS No. 506065.

APPENDIX: THE MINI-ORANGE SPECTROMETER

The basis of how our mini-orange works [55–57] is shown in the top left part of Fig. 9. Electrons (positrons) from the source are bent toward (away from) a cooled Si(Li) detector by the magnetic field generated by wedge-shaped permanent magnets arranged symmetrically around a cylindrical plug made of tungsten. This plug prevents photons and particles from reaching the Si(Li) directly. The magnets are made of $SmCo_5$ and come in two shapes which are shown in the top right part of Fig. 9. The electron transmission is determined by the number and type of magnets, the distance from the source to the front face of the mini-orange and the distance from the source to the Si(Li) detector, all of which can be varied. Each configuration can be classified by $A/B/C$, where A is the number of magnets, B is the distance from the source to the mini-orange front face, and C is the distance from the source to the Si(Li) detector (bottom part of Fig. 9). The distances are in mm. The transmission for each configuration must be determined empirically. Figure 9 shows a horizontal cross section through the whole apparatus. The mass-separated beam from a mass separator, in this case the GPS at ISOLDE, is deposited onto a tape, which is moved at predetermined intervals to place the accumulated activity in front of the mini-orange.

One of the principal features of this mini-orange system was that Barden [33] went to some effort to ensure that the front face of the Si(Li) detector stays clean, in other words, that chemical contaminants in the vacuum do not condense on the cold face of the detector. This was achieved by the arrangement shown schematically in the bottom part of Fig. 9. As stated above, the details of how this was done are given in his thesis. Here we describe only the essential elements of the apparatus. The main chamber housing the mini-orange, marked III in the figure, can be separated from the rest of the system by a valve marked V. The rest of the system is divided into two compartments marked I and II. In the former the Si(Li) detector sits on the end of a cold finger held at liquid N_2 temperatures during operation. A window of polyethylene, aluminized on both sides, with a thickness of 260 μg cm^{-2} separates I and II. The Si(Li) detector is only cooled down once the vacuum in I has reached 10^{-7} mbar. This vacuum is achieved in two steps. Initially a vacuum of 10^{-4} mbar

is established in the whole volume including I, II, and III using a standard cryopump system. At this point I and II are connected by another valve not shown in the figure. Once the vacuum of 10^{-4} mbar is reached, the valve connecting I and II is closed, an ion getter pump is started, and a cold trap on the pumping line to I is filled. Now the vacuum of 10^{-7} mbar is established in I and this compartment is kept isolated during the measurements. Because the window in front of the Si(Li) is fragile it is important that the vacuum in II is maintained throughout the measurements. This could be done with the help of valve V, which was closed every time the mini-orange chamber had to be opened.

[1] W. Gelletly, Il Nuovo Cimento **111A**, 757 (1998).
[2] C. J. Lister, P. J. Ennis, A. A. Chishti, B. J. Varley, W. Gelletly, H. G. Price, and A. N. James, Phys. Rev. C **42**, 1191 (1990).
[3] W. Gelletly *et al.*, Phys. Lett. B **253**, 287 (1991).
[4] R. F. Casten, Nucl. Phys. A **443**, 1 (1985).
[5] R. F. Casten, D. S. Brenner, and P. E. Haustein, Phys. Rev. Lett. **58**, 658 (1987).
[6] S. L. Tabor, Phys. Rev. C **34**, 311 (1986).
[7] R. B. Piercey *et al.*, Phys. Rev. Lett. **47**, 1514 (1981).
[8] C. Chandler *et al.*, Phys. Rev. C **56**, 2924(R) (1997).
[9] F. Becker *et al.*, Eur. Phys. J. A **4**, 103 (1999).
[10] E. Bouchez *et al.*, Phys. Rev. Lett. **90**, 082502 (2003).
[11] E. Clément *et al.*, Phys. Rev. C **75**, 054313 (2007).
[12] I. Hamamoto and X. Z. Zhang, Z. Phys. A **353**, 145 (1995).
[13] P. Sarriguren *et al.*, Nucl. Phys. A **635**, 55 (1998).
[14] E. Nácher *et al.*, Phys. Rev. Lett. **92**, 232501 (2004).
[15] E. Poirier *et al.*, Phys. Rev. C **69**, 034307 (2004).
[16] B. Rubio *et al.*, J. Phys. G: Nucl. Part. Phys. **31**, S1477 (2005).
[17] W. Nazarewicz *et al.*, Nucl. Phys. A **435**, 397 (1985).
[18] P. Bonche *et al.*, Nucl. Phys. A **443**, 39 (1985).
[19] M. Bender, P. Bonche, and P.-H. Heenen, Phys. Rev. C **74**, 024312 (2006).
[20] S. Hilaire and M. Girod, Eur. Phys. J. A **33**, 237 (2007).
[21] G. A. Lalazissis and M. M. Sharma, Nucl. Phys. A **586**, 201 (1995).
[22] A. Petrovici, K. W. Schmid, and A. Faessler, Nucl. Phys. A **605**, 290 (1996); **665**, 333 (2000).
[23] H. Grawel *et al.*, Z. Phys. A **341**, 247 (1992). Note that the correct name of the first author is H. Grawe but it appears as H. Grawel in this journal.
[24] J. Mukai *et al.*, Z. Phys. A **356**, 1038 (1996).
[25] J. H. McNeill *et al.*, Oak Ridge National Laboratory Progress Report, 1990, p. 63.
[26] R. A. Kaye *et al.*, Phys. Rev. C **54**, 1038 (1996).
[27] R. A. Kaye, L. A. Riley, G. Z. Solomon, S. L. Tabor, and P. Semmes, Phys. Rev. C **58**, 3228 (1998).
[28] P. Sarriguren, Phys. Rev. C **79**, 044315 (2009).
[29] H. L. Ravn *et al.*, Nucl. Instrum. Methods **123**, 131 (1975).
[30] R. Eder *et al.*, Nucl. Instrum. Methods B **62**, 535 (1992).
[31] C. F. Liang *et al.*, Z. Phys. A **309**, 185 (1982).
[32] E. Hagebø *et al.*, in *Proceedings of the Workshop Nuclear Structure of Light Nuclei Far from Stability, Experiment and Theory, Obernai, France, 1989*, edited by G. Klotz (Univ. Louis Pasteur, 1991), p. 241.
[33] R. Barden, Ph.D. thesis, Johannes-Gutenberg Universitaet Mainz, 1988.
[34] C. J. Lister *et al.*, Phys. Rev. C **28**, 2127 (1983).
[35] C. J. Lister, P. E. Haustein, D. E. Alburger, and J. W. Olness, Phys. Rev. C **24**, 260 (1981).
[36] J. Liptak and J. Kristiak, Nucl. Phys. A **311**, 421 (1978).
[37] T. Kibédi *et al.*, Nucl. Instrum. Methods A **589**, 202 (2008).
[38] J. Gulyás, computer code ELEVEN (MTA Atomki, Debrecen, unpublished).
[39] N. B. Gove and M. J. Martin, Nucl. Data Tables A **10**, 205 (1971).
[40] J. C. Hardy and I. S. Towner, Phys. Rev. C **79**, 055502 (2009).
[41] G. Audi *et al.*, Nucl. Phys. A **729**, 337 (2003).
[42] P. M. Endt, At. Data Nucl. Data Tables **23**, 547 (1979).
[43] C. Ekström, S. Ingelman, G. Wannberg, and M. Skarestad, Nucl. Phys. A **311**, 269 (1978).
[44] G. K. Bavaria, J. E. Crawford, S. Calamawy, and J. E. Kitching, Z. Phys. A **302**, 329 (1981).
[45] A. B. Pérez-Cerdán *et al.* (unpublished).
[46] J. C. Hardy, L. C. Carraz, B. Jonson, and P. G. Hansen, Phys. Lett. B **71**, 307 (1977).
[47] S. Raman and N. B. Gove, Phys. Rev. C **7**, 1995 (1973).
[48] C. J. Lister, B. J. Varley, H. G. Price, and J. W. Olness, Phys. Rev. Lett. **49**, 308 (1982).
[49] P. Möller, J. R. Nix, W. D. Myers, and W. J. Swiatecki, At. Data Nucl. Data Tables **59**, 185 (1995).
[50] F. Buchinger *et al.*, Phys. Rev. C **41**, 2883 (1990).
[51] C. Thibault *et al.*, Phys. Rev. C **23**, 2720 (1981).
[52] Balraj Singh, Nucl. Data Sheets **96**, 1 (2002).
[53] M. Keim *et al.*, Nucl. Phys. A **586**, 219 (1995).
[54] C. J. Gallagher Jr. and S. A. Moszkowski, Phys. Rev. **111**, 1282 (1958).
[55] J. van Klinken and K. Wisshak, Nucl. Instrum. Methods **98**, 1 (1972).
[56] J. van Klinken, S. J. Feenstra, K. Wisshak, and H. Faust, Nucl. Instrum. Methods **130**, 427 (1975).
[57] J. van Klinken, S. J. Feenstra, and G. Dumont, Nucl. Instrum. Methods **151**, 433 (1978).